Composites of ZnO nanoparticles and biomass based activated carbon: adsorption, photocatalytic and antibacterial capacities

G. J. F. Cruz, M. M. Gómez, J. L. Solis, J. Rimaycuna, R. L. Solis, J. F. Cruz, B. Rathnayake and R. L. Keiski

ABSTRACT

Composite material (AC-ZnO) was prepared by growing ZnO nanoparticles during the production of biomass based-activated carbon (AC) via the incorporation of zinc acetate in the process. Comprehensive analyses confirmed the presence of ZnO nanoparticles over the AC surface and described the particular nature of the composite adsorbent. Methylene blue (MB) equilibrium data fitted the Dubinin-Radushkevich model. The MB adsorption capacity was higher for the bare activated carbons (197.9–188.7 mg/g) than the activated carbons with ZnO nanoparticles (137.6–149.7 mg/g). The adsorption of the MB on the adsorbents is physical because the mean adsorption energy (E) is between 1.76 and 2.00 kJ/mol. Experiments that combine adsorption and photocatalysis were carried out with different loads of adsorbents and with and without UV-light exposure. Photocatalytic activity was identified mostly at the first stage of the adsorption process and, in the case of experiments with less load of the composite AC-ZnO, because the light obstruction effect of the activated carbon is more for higher loads. The ZnO grown over AC improves the adsorption of cations such as Pb, Al and Fe in aqueous phase (polluted river water) and provides antibacterial capacity against *Escherichia coli* and *Salmonella typhimurium*.

Key words | activated carbons, antibacterial nanoparticles, Dubinin-Radushkevich, photocatalysis, residual biomass, surface diffusion, water pollutants

G. J. F. Cruz (corresponding author)
J. Rimaycuna
Departamento de Ingeniería Forestal y Gestión Ambiental,
Universidad Nacional de Tumbes,
Av. Universitaria s/n, Campus Universitario – Pampa Grande, Tumbes,
Perú
E-mail: *gcruzc@untumbes.edu.pe*

M. M. Gómez
J. L. Solis
Facultad de Ciencias,
Universidad Nacional de Ingeniería,
Av. Tupac Amaru 210, Lima 25,
Perú

R. L. Solis
Departamento de Biología y Bioquímica,
Universidad Nacional de Tumbes,
Av. Universitaria s/n, Campus Universitario – Pampa Grande, Tumbes,
Perú

J. F. Cruz
Departamento de Química,
Universidad Nacional de Piura,
Campus Universitario – Miraflores s/n, Piura,
Perú

B. Rathnayake
R. L. Keiski
Faculty of Technology, Environmental and Chemical Engineering,
University of Oulu,
P.O.Box 4300, Oulu FI-90014,
Finland

INTRODUCTION

Currently, the pollution of rivers is one of the most important environmental concerns in developing countries. It is common to find pollutants such as heavy metals, dyes and fecal bacteria in the river waters caused by urban and industrial activities. Mining is the most common activity that introduces heavy metals into these aquatic ecosystems. As and Pb are considered as highly dangerous elements for humans due to their toxicity and easy transport through the trophic chain (Nagajyoti *et al.* 2010). Methylene blue (MB) is a common member of the group of pollutant dyes with wide application in textile, paper, cosmetic and paint industries. The effects of this compound include the disruption of biological processes such as photosynthesis in aquatic ecosystems (Copaciu *et al.* 2013). The main source of fecal bacteria as a water contaminant is sewage, which in rural and urban areas in developing countries is disposed into the rivers without treatment.

Adsorption with activated carbon (AC) is the most used commercial method of water and wastewater treatment, due to its efficiency and relatively low cost (Rafatullah *et al.* 2010;

doi: 10.2166/wst.2018.176

Hor *et al.* 2016). Activated carbon is commonly produced from coal. However, the use of coal is not sustainable and new renewable raw materials for AC production are needed. Agricultural residues have been used as raw materials for activated carbon production with adequate characteristics to be used in the adsorption of pollutants from water (Kadirvelu 2001; Sekar *et al.* 2004; Imamoglu & Tekir 2008; Singh *et al.* 2008; Tao & Xiaoqin 2008; Cruz 2012). AC produced from agricultural waste has a well-developed micro-mesoporous structure and good mechanical properties.

ZnO is a widely used nanoparticle in different applications, including water treatment, because of its photocatalytic and antibacterial properties. Some of the remarkable properties of this semiconductor material are its non-toxic nature and thermal stability (Saravanan *et al.* 2013). The photocatalytic property of ZnO has been demonstrated over a wide range of pollutants such as dyes (Rahman *et al.* 2013). Its antibacterial properties have been successfully studied over a wide range of bacteria strains (Manjunath *et al.* 2015). However, the major problem related to the use of ZnO nanoparticles in water treatment is the removal of the nanoparticles from the aqueous phase after the water treatment.

In that sense, the growth of ZnO onto the activated carbon would permit to obtain a composite material having combined or synergetic features such as high surface area, mechanical strength, thermostability and insolubility, antibacterial capacity and photocatalytic properties.

In this paper, composite adsorbent materials were produced and characterized based on activated carbons made from residual biomass (corn cob or red mombin seed) and nanoparticles of ZnO grown on the AC surface. Adsorption/photocatalytic combined experiments were carried out and the mechanisms were elucidated. Besides, studies of adsorption of heavy metals in real polluted water and antibacterial capacity against *Escherichia coli* and *Salmonella typhimurium* were conducted.

MATERIAL AND METHODS

Chemicals

Zinc acetate ($Zn(C_2H_3O_2)_2$) and zinc chloride ($ZnCl_2$) (both from Emsure ACS, ISO, Reag. Ph Eur – Merck) were used as chemical activation agents to produce activated carbons and as precursors for the production of ZnO nanoparticles, respectively. For the equilibrium and kinetic experiments 1,000 mg/L solution of MB (Certistain C.I. 52015 – Merck) was prepared.

Production of adsorbents

Activated carbons were produced from residual biomass of corn cob (*Zea mays*) and red mombin seed (*Spondias purpurea*) following the sequence introduced in previous works (Cruz *et al.* 2012, 2015; Pirila *et al.* 2017). These samples of activated carbon were codified such as CC and RMS from corn cob and red mombin seed, respectively.

To grow nanoparticles of ZnO on activated carbons, the raw materials were mixed with zinc chloride as the chemical activator and with zinc acetate dissolved in distilled water as the ZnO nanoparticles precursor in the proportion of 1/1/0.5 (wt/wt/wt). The mixture was dried at 80 °C overnight and then put in a ceramic tube to be carbonized in a metallic reactor inside a horizontal oven and heated at 600 °C for 2 h. The adsorbent material was subsequently washed with HCl solution (0.15 M) and rinsed with boiled and cooled distilled water. Washing and rinsing was repeated for several times with distilled water. Composites AC-ZnO were codified as: CC-ZnO and RMS-ZnO, for materials derived of corncob and red mombin seed, respectively.

Characterization of adsorbents

Textural parameters were calculated based on the information of the nitrogen physisorption isotherms performed by a Gemini VII 2390 Surface Area Analyzer (Micromeritics, USA). The specific surface area (S_{BET}) was calculated by the Brunauer, Emmett and Teller (BET) theory using the values of relative pressure (p/p_0) in the range between 0.05 and 0.25, the total pore volume (V_{net}) by using the data of nitrogen adsorption at the maximum value of p/p_0 (~0.9900) from the nitrogen adsorption branch, the micropore volume (V_{micro}) and the mesopore surface area (S_{meso}) by using the *t*-plot method with the Harkin-Jura equation. Pore size distribution (PSD) of the mesoporous region of the adsorbents was studied using the Barrett, Joyner and Halenda (BJH) method with the Jarkins and Jura equation. The pH of the point of zero charge (pH_{PZC}) of the samples was determined based on the pH drift method (Lopez-Ramon *et al.* 1999).

Morphology of the samples was studied using a field emission scanning electronic microscopy (FESEM) Zeiss Ultra Plus at different magnifications. The samples were coated with platinum before the analyses to obtain high quality pictures. Raman spectra of the materials were obtained using a high-resolution confocal μ-Raman system

Horiba Jobin-Yvon LabRAM HR800, while the structural analysis was carried out by a diffractometer Siemens D5000 operated at 30 kV and 20 mA.

Adsorption experiments

Equilibrium adsorption of methylene blue (MB)

Five MB solutions were prepared in distilled water having concentrations between 40 and 120 mg/L. 100 mL of each solution was placed in 250 mL flasks and 0.05 g of AC was added so that the concentration 0.5 g/L was kept for all the experiments. The flasks were shaken at 180 rpm in an orbital shaker during 48 h at a constant temperature of 30 ± 2 °C. The MB concentrations were measured on a Spectroquant Pharo 300 UV-VIS spectrophotometer (Merck) at 664 nm. Langmuir (1918), Freundlich (1906), Redlich & Peterson (1959) and Dubinin & Radushkevich (1947) models (Table 1) were used in modelling the equilibrium data. The models were used in the non-linear form and the parameters were calculated using the Solve tool of excel software and without depuration of any adsorption data. For all the models, the coefficient of determination (R^2) and the nonlinear chi-squared (χ^2) values were calculated (Tran *et al.* 2017).

MB kinetic adsorption/photocatalytic experiments

The MB kinetic experiments were conducted to test the combined adsorption/photocatalytic properties of the materials impregnated with ZnO nanoparticles. The experiments were conducted with and without a UV light without temperature modifications. The light source was a 300 W Ultra-Vitalux OSRAM sun lamp with UVA (13.6 W) and UVB (3 W). The initial MB concentration was 10 mg/L and three different composite ZnO-AC doses (0.1, 0.2 and 0.5 g/L) were tested. 200 mL of the suspensions were mixed (250 rpm) using a magnetic stirrer during the experiments in a chamber with irradiation of UV light and in a dark chamber. Different liquid aliquots were extracted and filtered (through a paper filter Whatman 41) at the beginning of the experiments and at different times between 5 and 300 min. The MB concentration was determined using a UV-VIS Perkin Elmer Lambda 25 at 664 nm. The pseudo-first-order (Lagergren 1898), pseudo-second order (Blanchard *et al.* 1984) and Elovich (Roginsky & Zeldovich

Table 1 | Equilibrium adsorption model (non-linear) and their respective parameters used in this study

Equilibrium models

Model	Equation		Parameters
Langmuir	$q_e = \frac{Q^0_{max} K_L C_e}{1 + K_L C_e}$	(1)	q_e = amount of adsorbate uptake at equilibrium (mg/g) C_e = adsorbate concentration at equilibrium (mg/L) Q^0_{max} = maximum saturated monolayer adsorption capacity of the adsorbent (mg/g) K_L = constant related to the affinity between adsorbent and adsorbate (L/mg)
Freundlich	$q_e = K_F C_e^n$	(2)	K_F = Freundlich constant (mg/g)/(mg/L)^n n = Freundlich intensity parameter (dimensionless)
Redlich-Peterson	$q_e = \frac{K_{RP} C_e}{1 + a_{RP} C_e^g}$	(3)	K_{RP} (L/g) and a_{RP} (mg/L)$^{-g}$ = Redlich-Peterson constants g = (dimensionless)
Dubinin-Radushkevich	$q_e = q_{DR} e^{-k_{DR} \varepsilon^2}$	(4)	q_{DR} = adsorption capacity (mg/g) K_{DR} = constant related to the sorption energy (mol^2/KJ^2) ε = Polanyi potential, calculated by the equation $\varepsilon = RT\ln(1 + 1/C_e)$, R is the of gas constant and T is temperature (kelvin) E = mean adsorption energy (kJ/mol) calculated by the equation $E = 1/(2\,K_{DR})^{1/2}$
Kinetic models			
Pseudo-first order	$q_t = q_e(1 - e^{-k_1 t})$	(5)	q_t = amount of adsorbate adsorb per mass of adsorbent at time t (mg/g) q_e = amount of adsorbate adsorb per mass of adsorbent at equilibrium (mg/g) k_1 = rate constant of the PFO equation (1/min)
Pseudo-second order	$q_t = \frac{q_e^2 k_2 t}{1 + k_2 q_e t}$	(6)	k_2 = rate constant of the PFO equation (g/mg x min) h = initial adsorption rate (mg/g x min), $h = k_2 q_e^2$
Elovich	$q_t = \frac{1}{\beta}\ln(1 + \alpha\beta t)$	(7)	α = initial rate constant (mg/g x min) β = desorption constant during experiment (mg/g)

1934) models (Table 1) were used to fit the adsorption data. The models were used in the non-linear form and the parameters were calculated using the Solve tool of Microsoft Excel software and without depuration of any adsorption data. The coefficient of determination (R^2) and the non-linear chi-squared (χ^2) values were calculated for all models.

Additionally, in order to study the rate limiting stage of the process and to understand the mechanism of the process, the intraparticle diffusion model (Weber & Morris 1963) was applied:

$$q_t = k_{diff}\sqrt{t} + C \quad (8)$$

where k_{diff} ($mg/g \times min^{1/2}$) is the rate constant of the intraparticle diffusion model and C (mg/g) is a constant associated with the thickness of the boundary layer.

Adsorption of As and Pb from the Tumbes River water

Kinetic experiments were performed with real polluted water to test mainly the As and Pb adsorption capacity of the activated carbons and the composite ZnO-AC. A sample of polluted river water was taken from the Tumbes River in Peru during the wet season (January) and adequately preserved until the experiments. Different aliquots were taken at the beginning and at different times between 5 and 300 min with a 10 mL syringe. The aliquots were filtered to retain activated carbon particles and then acidified with nitric acid p.a. until pH was below 3.

Besides As and Pb, other elements such as Al, Fe were determined in the initial river water sample and at the end of the kinetic experiments after 300 min to study the effect of the adsorbents over other cations in the river water. Heavy metals concentrations were determined using an Inductively Coupled Plasma Mass Spectrometer, Thermo Fisher Scientific, XSeries II QICP-MS.

Antibacterial activity

The antibacterial activity of the samples against *E. coli* (ATCC 25922) and *S. typhimurium* (ATCC 14028) was determined. The bacteria were grown in Luria broth at 36 ± 1 °C during 24 h. Then an aliquot of the culture was suspended in a physiological saline solution (10 mL) and the turbidity was adjusted to 0.5 of the MacFarland nephelometer (1×10^8 CFU/mL). 0.1 g of the adsorbents (AC and composite ZnO-AC) was added into the suspension and then it was stirred during 2 h at room temperature. 0.1 mL of the suspension was taken at different times between 0 and 140 min and then diluted. The diluted solution was seeded with 20 mL of Muller-Hinton agar and it was incubated at 37 °C for 24 h. Then, the percentage of dead cells relative to the growth control was calculated by determining the number of living cells (CFU/mL) of each tube using the agar plate count method (Zhang *et al.* 2004; Ortiz-Ibarra *et al.* 2007; Srinivasan *et al.* 2013).

RESULTS AND DISCUSSION

Adsorbents characterization

The shape of the nitrogen adsorption isotherms of the samples revealed that the activated carbons and composite ZnO-activated carbons are mainly microporous materials (isotherm type I according to IUPAC), however, the presence of hysteresis loop indicates a mesoporous structure as well (Figure 1(a)). Thus, all the samples have a microporous-mesoporous structure.

Table 2 shows the values of specific surface area, mesopore surface area, total pore volume, mesopore volume, the relationships S_{meso}/S_{BET} and V_{micro}/V_{net} and pH of the point of zero charge of the samples. The growth of ZnO over the activated carbon caused the values of S_{BET}, S_{meso}, V_{net} and V_{micro} to decrease, due that the ZnO growth on the surface was closing some pores of the activated carbons. Besides, the specific surface area of the ZnO was lower than those of the activated carbons, so the composite AC-ZnO has lower surface area than the bare AC (Han *et al.* 2011). The ratio S_{meso}/S_{BET} decreased and the ratio V_{micro}/V_{net} increased for AC-ZnO compared to the bare activated carbons. Additionally, the PSD is shown in Figure 1(b) and the amount of pores in the range of particle size between 2 and 50 nm (mesoporous region) decreases for the composite AC-ZnO in respect to the bare AC. It is evident that most of ZnO NPs occupied mesoporosity, while the microporosity is occupied to a lesser extent. It could be a negative factor during the adsorption of pollutants in aqueous phase, since higher mesoporosity improves the diffusion of pollutants through the pore structure of the solid phase.

In the case of the composites AC-ZnO, the pH_{PZC} of CC-ZnO (5.8) is slightly lower than the pH_{PZC} of the bare activated carbon (6.9), while for the sample RMS-ZnO, the value was similar to the bare activated carbon (6.8).

It is possible to notice from the X-ray diffractograms (Figure 2(a) and 2(b)), that all samples show two very broad peaks at 2θ around 21° and 42°. Those broad peaks

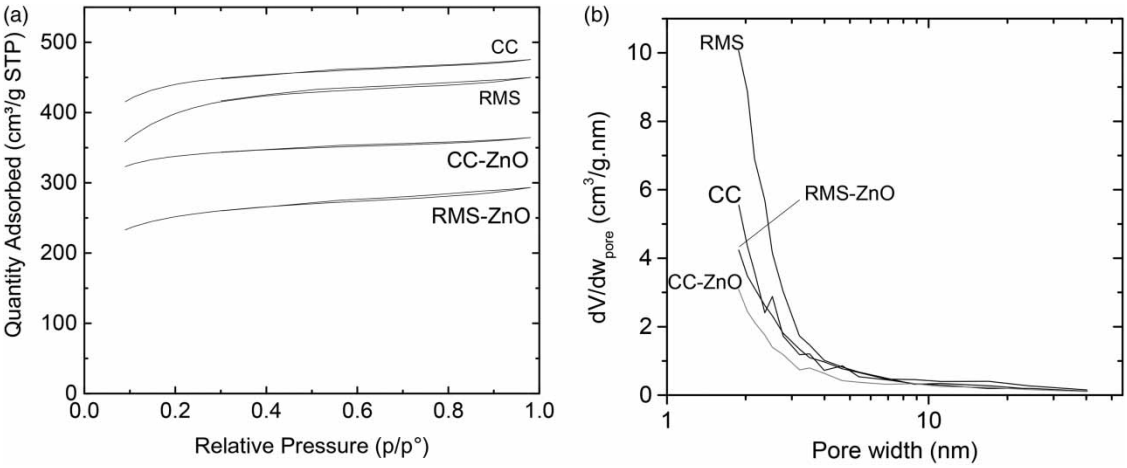

Figure 1 | Nitrogen adsorption isotherms at − 77 °C (a) and pore size distribution (b) of the studied samples.

could be assigned to (002) and (101) planes of the disordered graphite, which is common for the structure of an activated carbon (Acharya *et al.* 2009). Additional peaks that correspond to the ZnO (Z) and quartz (S) phases are identified in the diffractograms of the bare activated carbons (CC and RMS) (Figure 2(a)). The peaks of these additional phases from the RMS sample have higher intensities than the peaks from CC, thus, the concentration of those impurities are higher in the RMS sample than in CC. ZnO evolved from the chemical activator $ZnCl_2$ during the carbonization process in the activated carbon production and the quartz originated from the carbonization of the raw materials. Both composites (CC-ZnO and RMS-ZnO) have clear peaks assigned to the ZnO phase (Figure 2(b)).

Figure 2(c) and 2(d) show the Raman spectra of the studied adsorbents. Two centered bands were identified for all the samples. The bands at around 1,600 cm^{-1} and 1,350 cm^{-1} correspond to G-band and D-band, respectively. G-band is labelled as a graphitic band, while D-band is labelled as a disorder band. Those bands are typical for activated carbons (Chu & Li 2006) and describe the amorphous character of the prepared samples dominated by nanocrystalline forms. The ratio of the intensity of the D-band (I_D) to the G-band (I_G) for composite samples AC-ZnO (I_D/I_G is equal to 0.93 and 0.92 for CC-ZnO and RMS-ZnO, respectively) corresponds to a more disordered structure than the bare samples (I_D/I_G is equal to 0.90 and 0.76 for CC and RMS, respectively). Apparently, the presence of ZnO over the activated carbon causes disorder in the AC structure. In the case of CC-ZnO, there are additional bands at around the wavenumber of 1,100 and/or 570 cm^{-1} which could be assigned ZnO.

Figure 3(a) and 3(d) show the FESEM micrographs of the bare activated carbon samples. CC and RMS have a porous surface with some impurities that might be pieces of the porous walls that are produced during the milling process of the activated carbon. Tetrahedral rods of ZnO are also shown in the surface of both bare ACs, due to the oxidation of $ZnCl_2$ used during the activation. This fact was confirmed by the XRD analysis (Figure 2(c)). In the FESEM micrographs of both activated carbon and composites AC-ZnO (Figure 3(b) and 3(c) for CC-ZnO and Figure 3(e) and 3(f) for RMS-ZnO), the pores are partially blocked by ZnO nanoparticles, i.e. the samples without modification have larger total specific surface area and total pore volume than the impregnated samples. Similar

Table 2 | Textural properties (S_{BET}, V_{net}, V_{micro}) and pH of zero charge (pH_{PZC}) of the samples

Parameter	S_{BET} (m^2/g)	S_{meso} (m^2/g)	S_{meso}/S_{BET} (%)	V_{net} $(cm^3/g)_{liq}$	V_{micro} $(cm^3/g)_{liq}$	V_{micro}/V_{net} (%)	pH_{PZC}
CC	1247.4	380.0	30.5	0.74	0.51	68.9	6.9
CCmod	947.9	230.4	24.3	0.56	0.42	75.0	5.8
RMS	1194.7	661.4	55.4	0.70	0.32	45.7	6.8
RMSmod	734.3	309.3	41.61	0.45	0.25	55.6	6.8

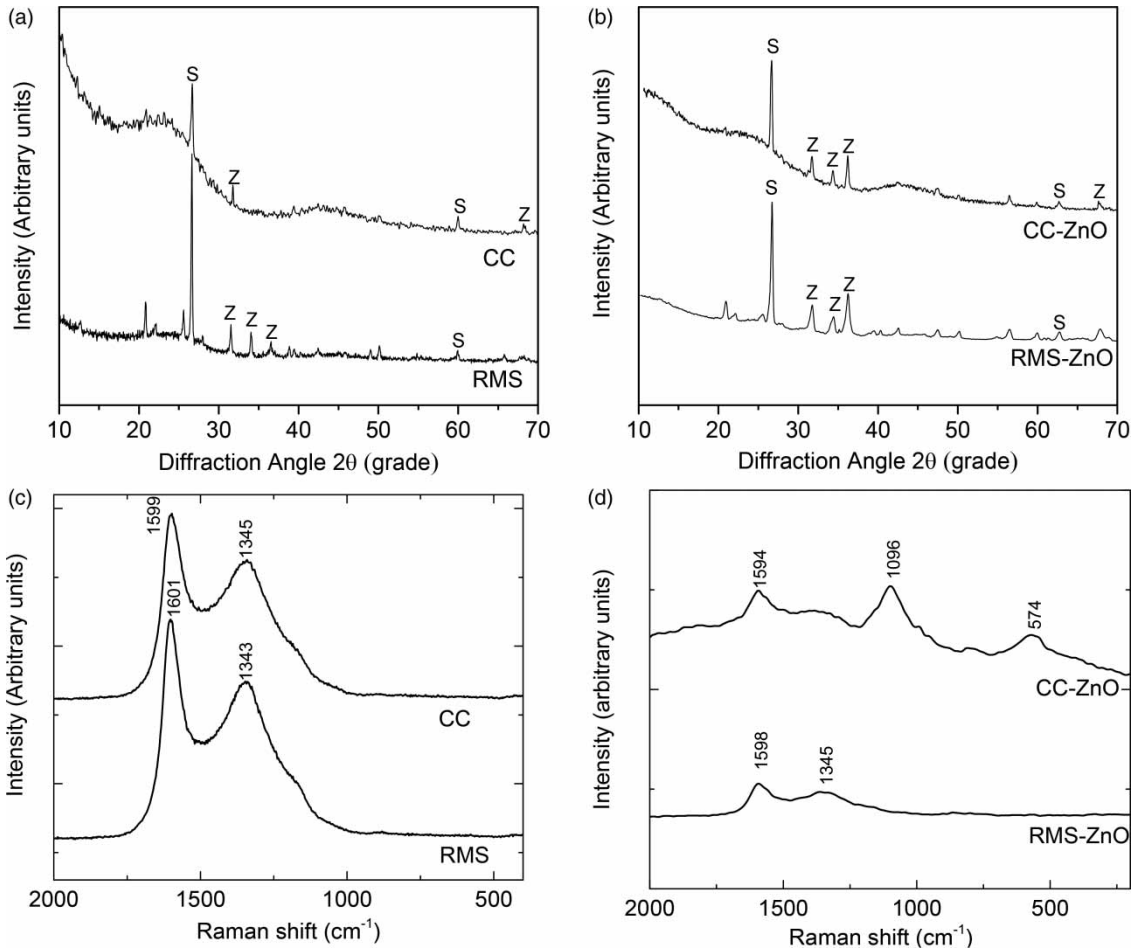

Figure 2 | XRD (a), (b) and Raman (c), (d) spectra of the produced adsorbents.

results were found by Sobana & Swaminathan (2007). It is possible to observe in Figure 3(c) that the CC-ZnO sample has some kind of a foam structure, whereas the RMS-ZnO sample (Figure 3(f)) has the tetrahedral rod morphology due to the presence of ZnO. ZnO grows as hexagonal rods with a radius of around 800 nm at the most and the length was some microns. As a comparison, bases have regular or irregular hexagonal structures.

Adsorption experiments

Equilibrium adsorption of MB

Table 3 shows the equilibrium parameters for the adsorption of methylene blue for the produced materials according to the different models used. Analyzing the values of R^2 and X^2 for each model, the equilibrium adsorption data of the samples CC ($R^2 = 0.93$, $X^2 = 4.95$), CC-ZnO ($R^2 = 0.97$, $X^2 = 0.64$) and RMS ($R^2 = 0.93$, $X^2 = 3.99$) fitted best the Dubinin-Radushkevich model, while the data from the sample RMS-ZnO fitted best the Redlich-Peterson model. Although the sample CC-ZnO has the highest value of R^2 (0.98) and lowest value of X^2 (0.44) for Redlich-Peterson model, this model is not correct because the value of g must not be higher than 1 (Tran *et al.* 2017).

The parameters of the Redlich-Peterson model for the equilibrium data of the sample RMS-ZnO were $K_{RP} = 594.31$ L/g and $a_{RP} = 5.29$ $(mg/L)^{-g}$ and $g = 0.88$. It means that K_{RP} is higher than 1 and a_{RP} is relatively close to 1 so that the Redlich-Peterson can be transformed into the Freundlich equation. This is the reason that explains that the Freundlich model fitted pretty well the equilibrium data of this sample. The heterogeneity of the RMS-ZnO surface due to the presence of ZnO nanorods over the carbon surface as it was shown in the FESEM micrographs could be the reason why this sample fitted well with the Freundlich model.

Based on the facts that most of the samples fitted best the Dubinin-Radushkevich model and the Redlich-Peterson

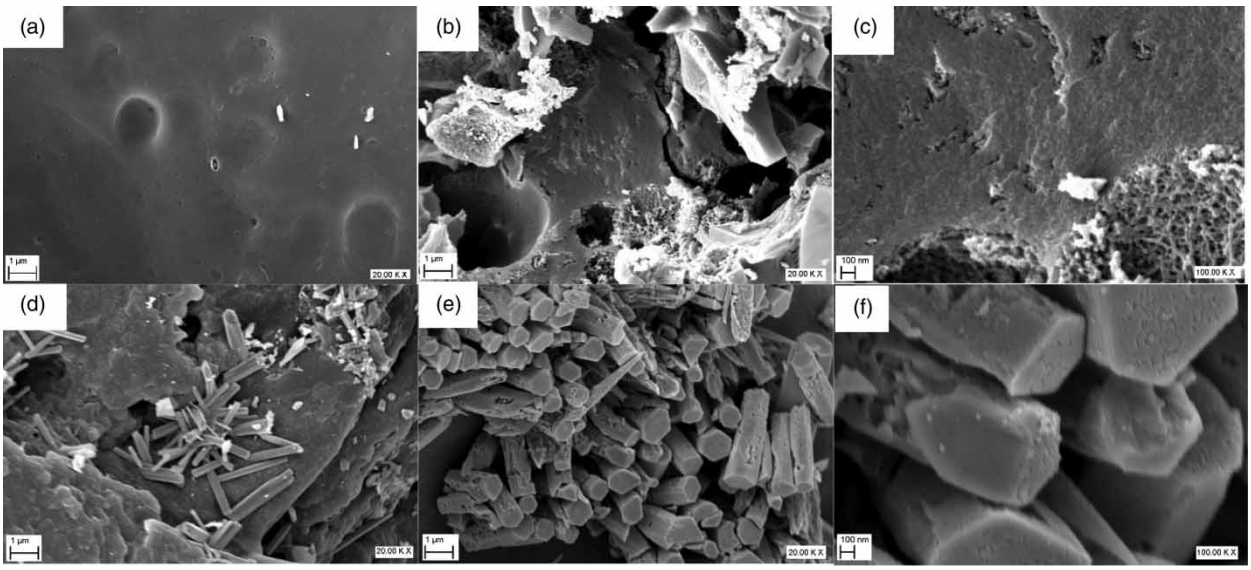

Figure 3 | FESEM micrographs of the produced samples: activated carbon made of corncob, CC (a), composite activated carbon made of corncob and ZnO nanoparticles, CC-ZnO (b), (c), activated carbon made of red mombin seed, RMS (d), composite activated carbon made of red mombin seed and ZnO nanoparticles, RMS-ZnO (e), (f).

model gives values that are not correct for the adsorption capacity of methylene blue at equilibrium, so the value of q_{DR} for the Dubinin-Radushkevich model will be taken into account to compare the materials. Bare activated carbons have higher adsorption capacities of methylene blue (197.91 and 188.7 mg/g of CC and RMS, respectively) than the AC-ZnO composites (137.6 and 149.7 mg/g for CC-ZnO and RMS-ZnO, respectively). This is because the surface areas of the bare activated carbons are higher than for the AC-ZnO composites. The lower S_{BET} of the composites samples than for the bare activated carbons means could be due that the reduction of the active adsorption sites on the carbon surface has an effect on its ability to adsorb MB.

The mean adsorption energies, E, are lower than 8 kJ/mol, and are between 1.76 and 2.00 kJ/mol, so the adsorption of methylene blue by the samples is predominantly physical. Ansari *et al.* (2016) and Pirsaheb *et al.*

Table 3 | Equilibrium models for the adsorption of methylene blue experiments

Model	Parameter	CC	CC-ZnO	RMS	RMS-ZnO
Langmuir	Q_{max} (mg/g)	206.7	141.4	194.8	154.9
	K_L (L/g)	1.65	1.46	1.76	1.44
	R^2	0.85	0.93	0.83	0.95
	X^2	11.19	1.49	10.76	1.25
Freundlich	K_F (mg/g)/(mg/L)^n	125.2	92.0	124.1	86.3
	n	0.17	0.11	0.14	0.17
	R^2	0.69	0.68	0.60	0.99
	X^2	20.97	7.48	22.87	0.42
Redlich-Peterson	K_{RP} (L/g)	259.8	145.7	230.06	549.31
	a_{RP} (mg/L)$^{-g}$	0.98	0.76	0.81	5.29
	g	1.09	1.09	1.13	0.88
	R^2	0.87	0.98	0.89	0.99
	X^2	9.35	0.44	6.96	0.14
Dubinin-Radushkevich	q_{DR} (mg/g)	197.9	137.6	188.7	149.7
	K_{DR} (mol^2/kJ^2)	0.13	0.16	0.13	0.13
	E (kJ/mol)	2.00	1.76	1.99	1.98
	R^2	0.93	0.97	0.93	0.93
	X^2	4.95	0.64	3.99	1.97

(2015) found a similar result for activated carbon samples as adsorbent and methylene blue as adsorbate and when ZnO nanorods loaded on activated carbon was used as adsorbent and bromocresol green and eosin dyes were used as adsorbates.

MB kinetic adsorption/photocatalytic experiments

In Figure 4(a)–4(f), q_t vs t curves of the MB kinetic adsorption/photocatalytic experiments are showed for the samples based on the used biomasses (corn cob and red mombin

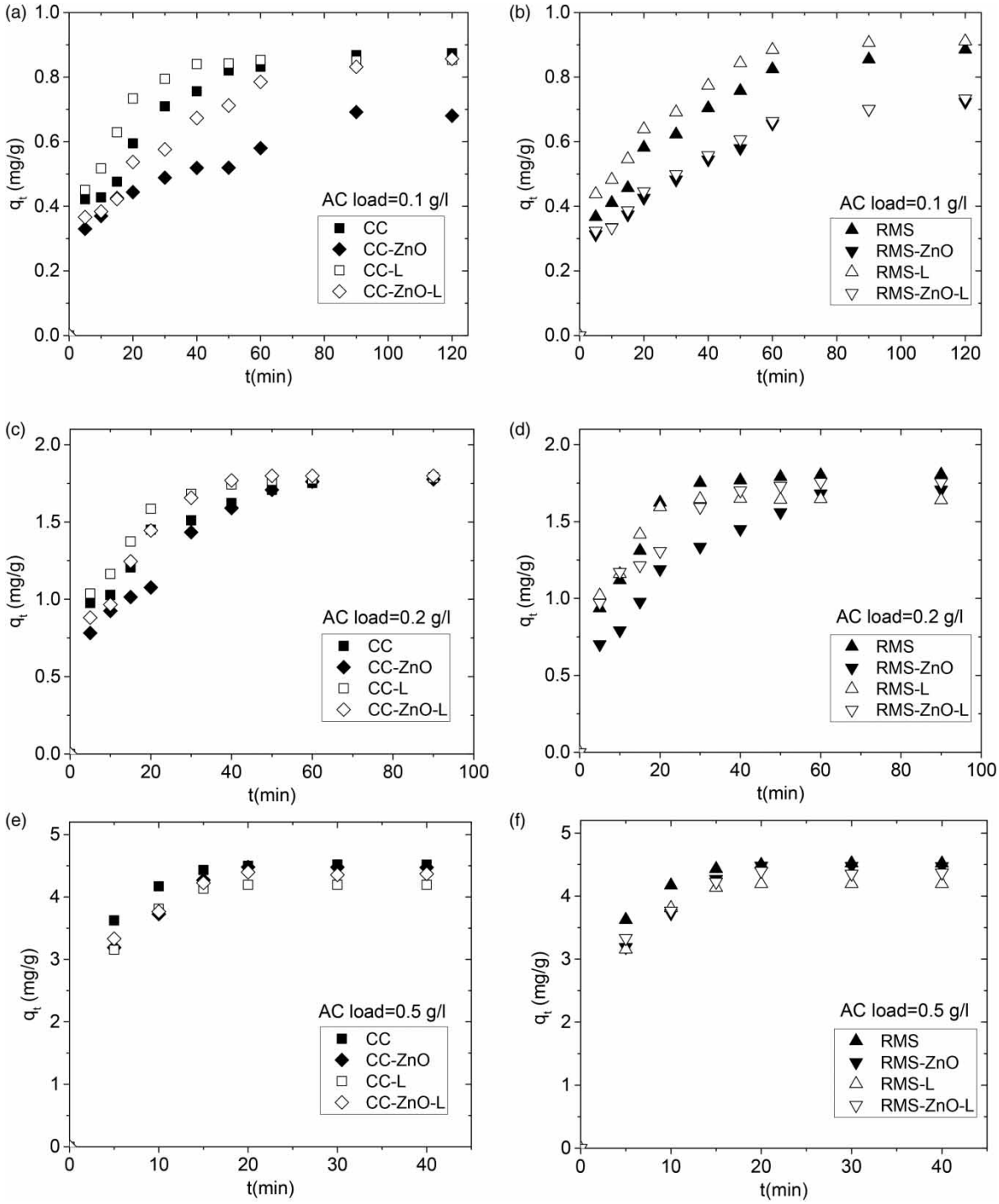

Figure 4 | Methylene blue kinetic adsorption/photocatalytic experiments with different activated carbon doses, with and without UV light.

seed) and the different activated carbon loads (0.1, 0.2 and 0.5 g/L). In order to identify the different experiments performed with the light irradiation and those conducted in darkness, the letter-L was added to the code of the experiments with light exposure. Simple preliminary experiment was conducted with light and without adsorbent, in order to take into account the influence of the light on the MB degradation.

The adsorption capacities of the samples evaluated with the presence of light are higher than for the samples evaluated without light. However, that behavior is more noticeable when the load of activated carbon is lower. This tendency will be explained in the next section.

Intraparticle model. Intraparticle kinetic modelling considering three stages of the adsorption process, i.e. surface diffusion, intraparticle diffusion and kinetic adsorption was used to evaluate the rate limiting stage of the adsorption. Every stage was analyzed individually using the model in order to evaluate the influence of the photocatalytic process. The graphics q_t vs $t^{0.5}$ for the intraparticle model are depicted in Figure 5(a)–5(f) for the samples with different initial loads of the produced adsorbents with and without the UV light exposure. The three stages of the process in all experiments were identified and separated by dotted lines. Table 4 shows the intraparticle model parameters. The parameters of the model were identified with the numbers 1, 2 and 3 for every stage, surface diffusion, intraparticle diffusion and equilibrium adsorption, respectively.

The first stage occurs very fast within the first 5 min for all samples. This first stage is fast because when the load of activated carbon is higher, the amount of active adsorption sites that can be occupied by the adsorbate is higher as well. The value of k_{diff1} for the experiments with light exposure is always higher than for the experiments without light exposure in the case of different loads of activated carbon. Only in the case of the experiment for the sample RMS with 0.5 g/L of activated carbon load, the value of k_{diff1} decreased for the experiment with the light exposure. In the second and third stage (intraparticle diffusion and equilibrium adsorption), k_{diff2} and k_{diff3} did not follow the k_{diff1} behavior, because these stages take place in the internal part of the adsorbents where the UV light cannot access. The UV light could reach the surface of the adsorbents, so the photocatalytic reactions can occur during the surface diffusion stage. On the other hand, the presence of high amount of activated carbon, as in the 0.5 g/L activated carbon load, could block the UV light disrupting the photocatalytic process in the surface diffusion stage.

Kinetic adsorption models. The parameters of the different applied models are shown in Table 5. When the load of activated carbon is increased, the applied model fitted better with the kinetic data. This fact is due to the fact, as it is possible to see in Figure 4(e) and 4(f) in the experiments carried out using 0.5 g/L of activated carbon, that the equilibrium is reached in a shorter time, clearly showing the three stages of the adoption process. However, in the case of the experiments carried out using 0.1 g/L and 0.2 g/L of activated carbon, the equilibrium is not reached or it is starting to be reached for most of the curves. The effectiveness related to the application of those kinetic models depends on the availability of data that includes the three stages of the adsorption process (Tran *et al.* 2017). Taking these into account, analyzing only the kinetic experiments where 0.5 mg/L of activated carbon was used, the model that best explains the data is the PSO model with the values of R^2 between 0.98–0.99 and X^2 between 2.54×10^{-5} – 0.01. The PFO and Elovich models are not good at explaining the kinetic parameters.

In most of the cases, the values of the initial adsorption rate h for the PSO model for the experiments where the load of activated carbon was 0.1 and 0.2 g/L were higher with the exposure of UV light, bearing out the explanation of the combined effect of adsorption and photocatalysis at the first stage of the process (surface diffusion).

Adsorption of As and Pb dissolved in the Tumbes River water

Since the adsorption of As and Pb was very fast by the samples and the adsorption equilibrium was reached in the earlier stages of the experiments with the Tumbes River water, only the adsorption data of the first 60 min was used in the experiment. The initial concentration of heavy metals and other elements in the river water are shown in Table 6.

Figure 6(a)–6(d) show the removal efficiency of As from the polluted river water using both bare ACs and impregnated AC-ZnO. Close to 100% of As removal was reached during the first 5 min. Almost similar behavior was observed with the composites CC-ZnO and RMS-ZnO. In the case of Pb adsorption, the samples CC-ZnO and RMS-ZnO had better adsorption capacities than their respective bare activated carbons.

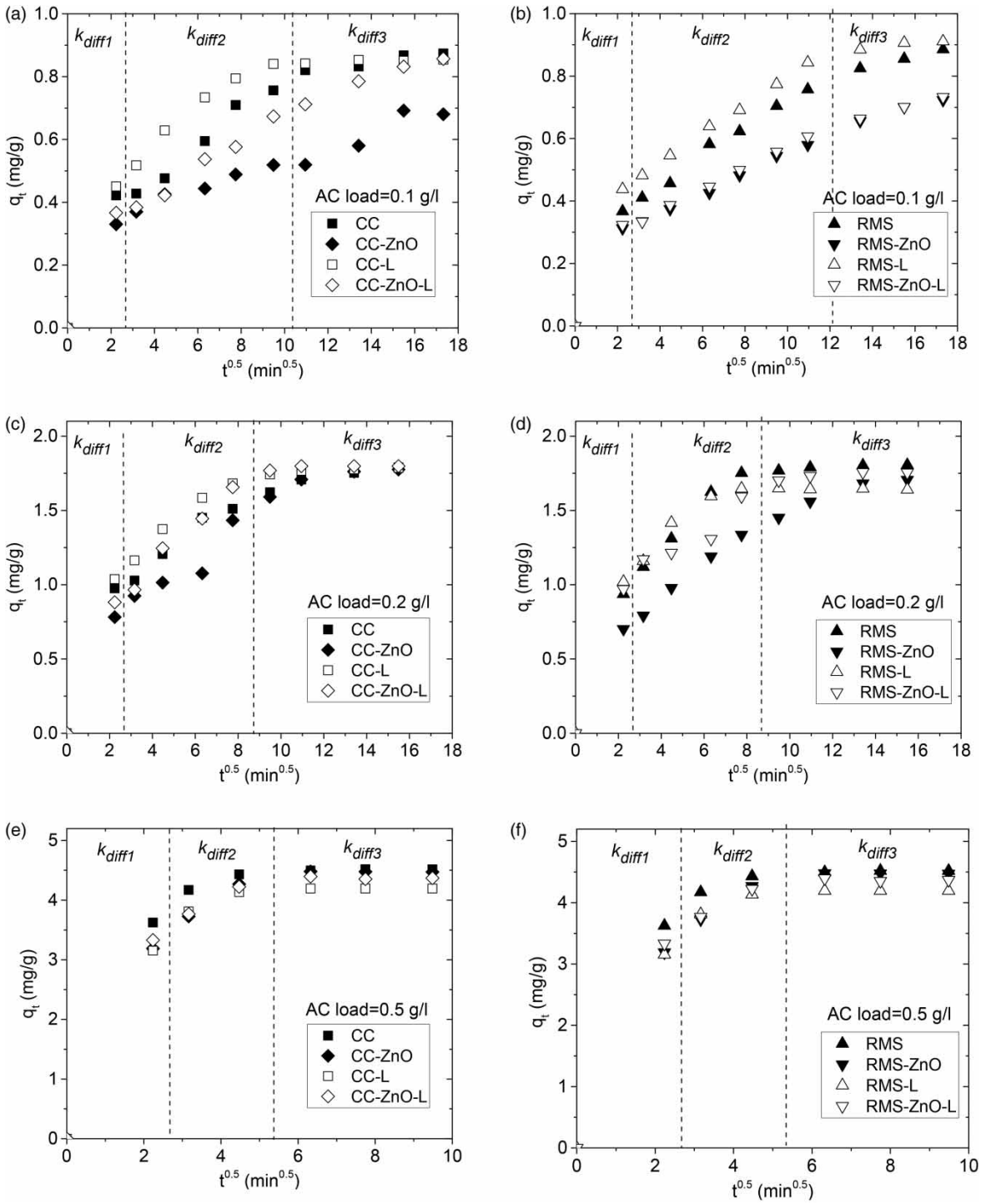

Figure 5 | Intraparticle diffusion model applied to the kinetic adsorption/photocatalytic experimental data.

The behavior of pH during the experiments with the bare samples was different according to the used biomass. RMS increases the pH from the initial pH of 5.7 to 6.5 at the first stage of the process and then this level is kept, while CC kept the pH value at 5.8. With respect to the pH behavior during the adsorption experiments with the composites AC-ZnO, the pH of both samples increased immediately at the beginning of the experiment (from 5.8)

Table 4 | Intraparticle diffusion model of the different stages of the adsorption/photocatalytic experiments

Parameter	CC	CC-L	CC-ZnO	CC-ZnO-L	RMS	RMS-L	RMS-ZnO	RMS-ZnO-L
Activated carbon load 0.1 g/L								
k_{Diff1} $(mg/g \cdot min^{-0.5})$	8.0×10^{-2}	9.0×10^{-2}	6.6×10^{-2}	7.3×10^{-2}	7.3×10^{-2}	8.8×10^{-2}	6.3×10^{-2}	6.5×10^{-2}
C_1 (mg/g)	7.0×10^{-17}	0	0	7×10^{-17}	0	0	0	0
R_1^2	1	1	1	1	1	1	1	1
k_{Diff2} $(mg/g \cdot min^{-0.5})$	3.7×10^{-3}	6.1×10^{-3}	2.6×10^{-3}	3.1×10^{-3}	3.4×10^{-3}	3.4×10^{-3}	2.4×10^{-3}	2.5×10^{-3}
C_2 (mg/g)	0.42	0.46	0.34	0.37	0.39	0.46	0.32	0.33
R_2^2	0.95	0.93	0.89	0.96	0.94	0.96	0.97	0.97
k_{Diff3} $(mg/g \cdot min^{-0.5})$	3.0×10^{-4}	6.0×10^{-5}	9.0×10^{-4}	8.0×10^{-4}	7.0×10^{-4}	4.0×10^{-4}	8×10^{-4}	7×10^{-4}
C_3 (mg/g)	0.78	0.84	0.43	0.63	0.69	0.81	0.50	0.53
R_3^2	0.93	0.76	0.92	0.95	0.95	0.88	0.94	0.98
Activated carbon load 0.2 g/L								
k_{Diff1} $(mg/g \cdot min^{-0.5})$	0.19	0.21	0.16	0.18	0.19	0.20	0.14	0.19
C_1 (mg/g)	1×10^{-16}	1×10^{-16}	0	0	1×10^{-16}	0	0	1×10^{-16}
R_1^2	1	1	1	1	1	1	1	1
k_{Diff2} $(mg/g \cdot min^{-0.5})$	7.7×10^{-3}	6.0×10^{-3}	9.3×10^{-3}	8.0×10^{-3}	4.8×10^{-3}	9.7×10^{-3}	8.8×10^{-3}	8.1×10^{-3}
C_2 (mg/g)	1.01	1.18	0.79	0.99	1.21	1.06	1.74	1.02
R_2^2	0.90	0.80	0.95	0.86	0.65	0.83	0.93	0.93
k_{Diff3} $(mg/g \cdot min^{-0.5})$	6.0×10^{-4}	2×10^{-6}	7.0×10^{-4}	2.0×10^{-4}	1.0×10^{-4}	1.2×10^{-3}	2.0×10^{-4}	1.0×10^{-4}
C_3 (mg/g)	1.65	1.79	1.63	1.75	1.78	1.43	1.71	1.67
R_3^2	0.90	0.75	0.99	0.99	0.88	0.87	0.65	1
Activated carbon load 0.5 g/L								
k_{Diff1} $(mg/g \cdot min^{-0.5})$	0.64	0.82	0.64	0.67	0.72	0.63	0.63	0.67
C_1 (mg/g)	0	6×10^{-16}	0	0	6×10^{-16}	6×10^{-16}	6×10^{-16}	0
R_1^2	1	1	1	1	1	1	1	1
k_{Diff2} $(mg/g \cdot min^{-0.5})$	5.3×10^{-2}	4.7×10^{-3}	6.9×10^{-2}	7.0×10^{-2}	5.0×10^{-2}	6.1×10^{-2}	7.0×10^{-2}	5.8×10^{-2}
C_2 (mg/g)	3.83	1.08	2.97	3.4	3.49	2.99	2.91	3.10
R_2^2	1	0.82	0.94	0.90	0.85	0.86	0.97	0.97
k_{Diff3} $(mg/g \cdot min^{-0.5})$	2.0×10^{-4}	1.0×10^{-4}	3.3×10^{-3}	7.0×10^{-4}	4.0×10^{-4}	9.0×10^{-4}	2.0×10^{-4}	2.1×10^{-4}
C_3 (mg/g)	4.41	4.17	4.26	4.45	4.49	4.12	4.49	4.19
R_3^2	0.52	0.41	0.82	0.93	0.56	0.82	0.99	0.89

Parameters with the number 1 correspond to the stage of surface diffusion, with number 2 correspond to intraparticle diffusion and with number 3 correspond to equilibrium adsorption.

and then it stayed at a level between 6.5 and 6.8 for both samples CC-ZnO and RMS-ZnO. Those levels were slightly higher than in the case of bare activated carbons.

The pH levels during the experiments of CC and RMS were below the pH_{PZC} for both samples, supposing that the net charge of both bare activated carbons is positive (Fiol & Villaescusa 2008), while for the composites, the pH_{PZC} values were 5.8 and 6.8 for CC-ZnO and RMS-ZnO, respectively. The reduction in the pH_{PZC} of CC-ZnO respect to CC coincides with Kikuchi *et al.* (2006). Therefore, the net charge of CC-ZnO sample is negative and for the RMS-ZnO sample it is almost neutral. On the other hand, at the pH level of the experiments, As is present in the solution as negatively charged oxyanion As(V) (Smedley & Kinniburgh 2002). In the case of the samples CC, RMS and CC-ZnO, these facts explained the high adsorption of As. In the case of sample RMS-ZnO, the amphoteric nature of activated carbons would be implicated in the adsorption of As by this sample.

Table 6, besides the initial concentration of the elements in the Tumbes River water, shows the concentrations of the cations after 300 min, and the Peruvian water quality

Table 5 | Evaluation of the MB kinetic models for the adsorption/photocatalytic experiments

Parameter	CC	CC-L	CC-ZnO	CC-ZnO-L	RMS	RMS-L	RMS-ZnO	RMS-ZnO-L
Pseudo-first order								
Activated carbon load 0.1 g/L								
q_1 (mg/g)	0.84	0.84	0.59	0.80	0.83	0.87	0.67	0.68
K_1 (min^{-1})	0.07	0.11	0.09	0.06	0.06	0.08	0.06	0.06
R^2	0.88	0.94	0.70	0.87	0.89	0.86	0.83	0.84
X^2	0.14	0.04	0.12	0.18	0.131	0.13	0.17	0.16
Activated carbon load 0.2 g/L								
q_1 (mg/g)	1.69	1.74	1.74	1.80	1.80	1.64	1.64	1.70
K_1 (min^{-1})	0.10	0.13	0.06	0.09	0.11	0.15	0.07	0.11
R^2	0.86	0.92	0.89	0.94	0.95	0.94	0.93	0.85
X^2	0.16	0.07	0.24	0.10	0.06	0.04	0.14	0.14
Activated carbon load 0.5 g/L								
q_1 (mg/g)	4.41	4.17	4.50	4.48	4.48	4.19	4.44	4.32
K_1 (min^{-1})	0.52	0.79	0.23	0.27	0.32	0.27	0.23	0.27
R^2	0.99	0.99	0.97	0.99	0.99	0.99	0.97	0.97
X^2	4×10^{-5}	1.7×10^{-4}	0.03	6×10^{-3}	5.3×10^{-3}	3.5×10^{-3}	0.03	0.03
Pseudo-second order								
Activated carbon load 0.1 g/L								
q_e (mg/g)	0.87	0.87	0.60	0.82	0.85	0.88	0.67	0.68
K_2 (g/mg · min)	0.11	0.19	0.25	0.09	0.09	0.13	0.12	0.12
h	0.08	0.14	0.09	0.06	0.07	0.10	0.05	0.06
R^2	0.88	0.97	0.75	0.85	0.88	0.88	0.81	0.83
X^2	0.11	0.01	0.08	0.15	0.11	0.08	0.13	0.12
Activated carbon load 0.2 g/L								
q_e (mg/g)	1.75	1.81	1.77	1.86	1.87	1.70	1.70	1.74
K_2 (g/mg · min)	0.09	0.12	0.05	0.07	0.09	0.16	0.05	0.11
h	0.29	0.38	0.16	0.23	0.31	0.45	0.14	0.33
R^2	0.92	0.97	0.86	0.96	0.97	0.98	0.93	0.88
X^2	0.07	0.02	0.05	0.06	0.03	0.01	0.11	0.08
Activated carbon load 0.5 g/L								
q_e (mg/g)	4.47	4.19	4.73	4.67	4.64	4.36	4.67	4.52
K_2 (g/mg · min)	0.53	2.10	0.09	0.12	0.16	0.13	0.09	0.12
h	10.59	36.89	2.04	2.64	3.56	2.53	2.01	2.51
R^2	0.99	0.99	0.99	0.98	0.99	0.99	0.99	0.99
X^2	1.7×10^{-3}	2.54×10^{-5}	5.1×10^{-3}	0.01	4.0×10^{-3}	0.01	5.3×10^{-3}	4.9×10^{-3}
Elovich								
Activated carbon load 0.1 g/L								
α	0.23	0.83	0.26	0.14	0.23	0.4219	0.18	0.20
β	5.42	7.02	8.27	5.09	5.12	5.58	6.41	6.42
R^2	0.93	0.90	0.95	0.96	0.99	0.98	0.98	0.99
X^2	0.02	0.03	0.01	0.14	8.5×10^{-3}	7.0×10^{-3}	0.01	5.6×10^{-3}

(*continued*)

Table 5 | continued

Parameter	CC	CC-L	CC-ZnO	CC-ZnO-L	RMS	RMS-L	RMS-ZnO	RMS-ZnO-L
Activated carbon load 0.2 g/L								
α	0.98	2.11	0.32	0.64	1.18	5.28	0.29	1.17
β	3.00	3.37	2.23	2.53	2.91	4.27	2.30	3.11
R^2	0.96	0.94	0.95	0.93	0.91	0.87	0.98	0.95
X^2	0.02	0.03	0.04	0.06	0.06	0.05	0.02	0.03
Activated carbon load 0.5 g/L								
α	5.1×10^{5}	5.1×10^{25}	20.31	86.72	564.91	90.97	20.33	70.62
β	3.99	15.57	1.49	1.87	2.32	2.03	1.51	1.88
R^2	0.98	0.99	0.95	0.93	0.96	0.94	0.95	0.95
X^2	0.01	6×10^{-4}	0.04	0.04	0.02	0.03	0.04	0.03

standard – PSWQ (ANA 2015), as well. The initial concentrations of Al, As, Fe and Pb in the polluted water surpass the PSWQ, however, after adsorption, the concentrations of these elements are reduced below the PSWQ levels, with the exception of the final Al concentration with CC-Ch and RMS-Ch samples. CC-ZnO and RMS-ZnO reached a higher reduction in the Al and Fe concentrations after 300 min than the CC and RMS samples. Similar behavior was demonstrated and explained in the case of adsorption of the cationic Pb. The impregnation with ZnO improved the adsorption of cationic heavy metals in the multicomponent aqueous phase.

Table 6 | Heavy metal content of the Tumbes River water after 300 min experiments

Element (μg/L)	Initial water quality	Concentration after 300 min (μg/L)				NEQS[a] (μg/L)
		CC	CC-ZnO	RMS	RMS-ZnO	
Al	1750	43.7	13.9	11.2	18.4	200
As	56.7	0.46	1.0	0.64	0.58	10
B	93	127	130	118	122	500
Ba	72	70.8	61.2	67.3	66.9	700
Be	<0.1	<0.1	<0.1	<0.1	<0.1	4
Cd	2.2	0.76	0.91	0.86	1.3	3
Co	3.5	2.5	2.5	2.9	2.7	–
Cr	2.9	7.0	0.68	0.4	0.87	50
Cu	207	5.5	3	2.4	34.8	2000
Fe	2920	26.3	<5	<5	<5	1000
Hg	<0.2	<0.2	<0.2	<0.2	<0.2	2
Mn	229	226	223	228	226	400
Mo	0.5	1.4	0.69	0.56	0.56	–
Ni	4	1.8	2	1.5	3.5	25
Pb	224	3.8	0.69	0.98	0.64	50
Sb	10.9	6.5	6.6	6.7	6.6	–
Se	1.7	0.63	0.7	0.66	0.62	50
Sn	0.54	<0.1	<0.1	<0.1	<0.1	—
Tl	0.046	0.049	0.042	0.063	0.094	—
U	0.25	<0.02	<0.02	<0.02	<0.02	20
V	4.8	<0.3	3.5	<0.3	<0.3	100
Zn	272	1440	7810	7940	4130	5000

[a]Peruvian National environmental standard of water quality.
—Not found.

The initial concentration of Zn in the river water not surpassed the PSWQ, however, this concentration is increased during the adsorption experiments. The samples impregnated with ZnO surpass this standard after the adsorption experiments. The increase in the Zn concentration in the water is caused by the release of ZnO from the activated carbon surface to the aqueous phase.

Antibacterial activity

E. coli and *S. typhimurium* were selected in this study as reference bacteria because both are Gram negative enterobacteria (indicators of fecal contamination in water) and they exist usually in urban wastewater. All adsorbents (bare and composites) had the ability to reduce *E. coli* and *S. typhimurium* (Figure 7(a)–7(d)) at certain levels. All curves reached a maximum value of elimination (%) and then stay almost constant, except the CC with both bacteria.

Samples based on corn cob impregnated with ZnO have inevitably higher abatement capacity of both bacteria compared to the bare samples. The presence of a low amount of ZnO in the CC sample is responsible for the lower antibacterial capacity (close to 40%) of the bare samples.

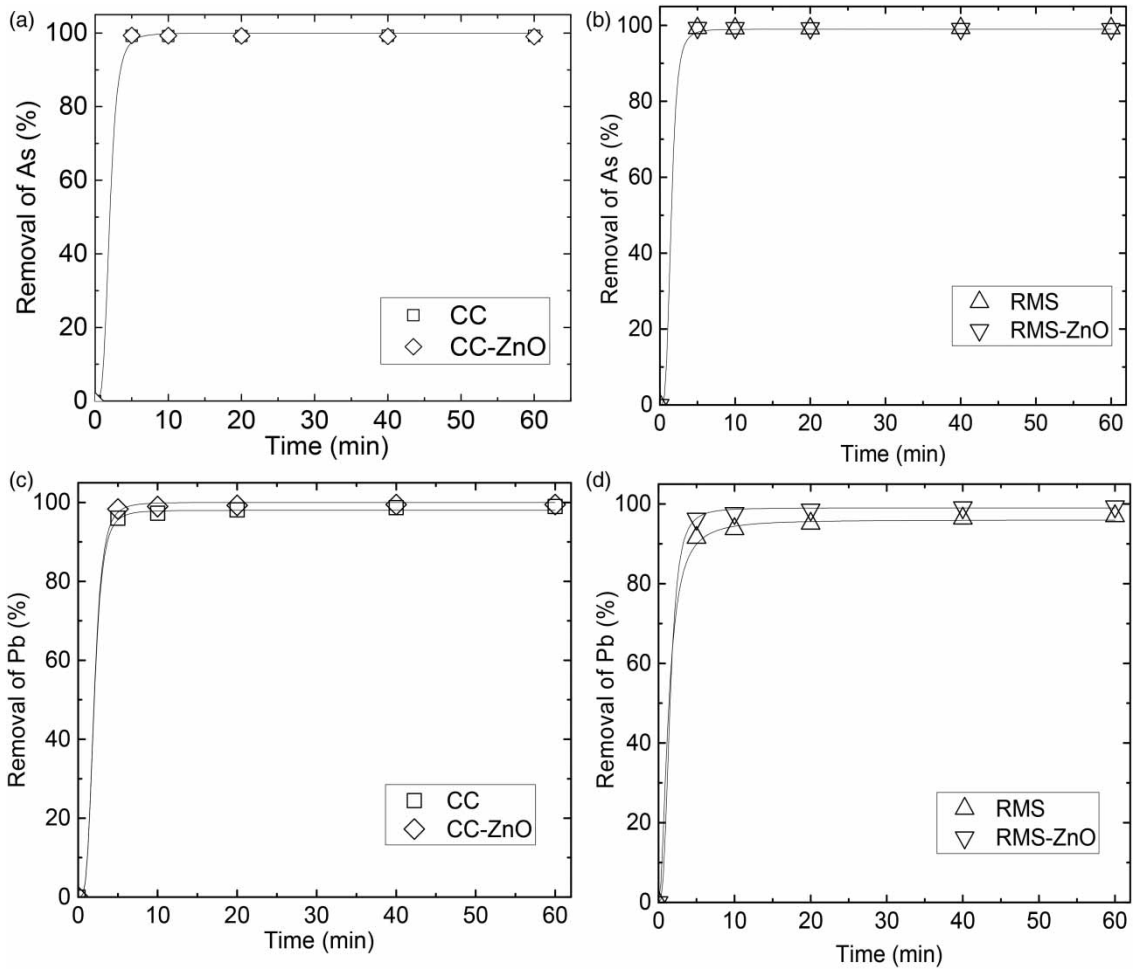

Figure 6 | Adsorption of As and Pb from polluted river water by the produced samples.

For the samples based on the red mombin seed, the difference in the antibacterial capacity of the bare and composite samples is not so visible. RMS-ZnO is slightly better than RMS. It is because the high content of ZnO evolved from the activator in the sample RMS.

It is evident that the presence of ZnO gave the adsorbents a good antibacterial activity.

CONCLUSIONS

Composite adsorbent materials were successfully prepared by growing ZnO nanoparticles during the production of activated carbon via the incorporation of zinc acetate in the process. ZnO nanoparticles over the activated carbon samples showed different sizes and morphologies according to the raw material used. In the case of corncob AC, a foam structure was created, whereas in the case of red mombin seed, ZnO nanorods were identified.

Adsorption capacity of adsorbents was tested with methylene blue (MB) as an adsorbent. MB equilibrium data fitted the best to the Dubinin-Radushkevich model with the adsorption capacity (q_{DR}) higher for the bare activated carbons (197.9–188.7 mg/g) than the activated carbons with ZnO nanoparticles (137.6–149.7 mg/g). The mean adsorption energy (E) (between 1.76–2.00 kJ/mol) led to the conclusion that the adsorption of MB on the adsorbents is physical.

Experiments that combine adsorption and photocatalysis were carried out with different loads of the adsorbents (0.1, 0.2 and 0.5 g/L) with and without UV light irradiation. Photocatalytic activity was identified mostly at the first stage of the adsorption process and in the case of experiments with a lower amount of AC because of the light obstruction effect of the activated carbon.

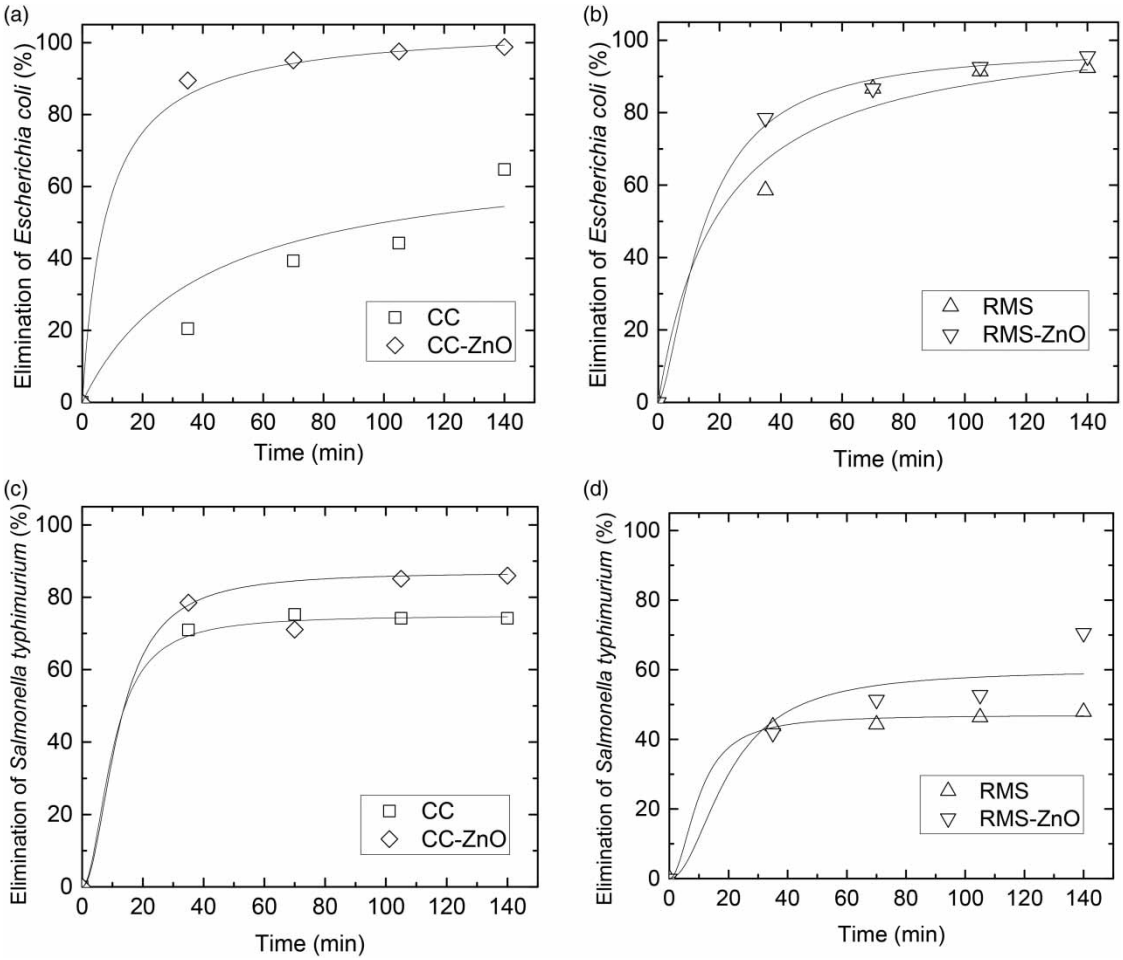

Figure 7 | Antibacterial activities of the prepared adsorbents over *E. coli* (ATCC 25922) and *S. typhimurium* (ATCC 14028).

The ZnO grown over AC improves the adsorption of cations such as Pb, Al and Fe in an aqueous phase (polluted river water) and provides the materials an antibacterial capacity against *E. coli* and *S. typhimurium*.

The composite materials are suitable materials for water treatment to eliminated chemical and microbial pollutants, further studies have to carry out in the sense of testing the materials in column experiments.

ACKNOWLEDGEMENTS

The Academy of Finland is acknowledged for research funding to the AdMatU project (DNo: 269631) from the Development funds. The National University of Tumbes (Proyecto Canon – Resolución N° 0722-2014/UNT-R) and the Peruvian National Council for Science and Technology (CONCYTEC) (Contract N° 024-2016-FONDECYT) are gratefully recognized for their support.

REFERENCES

Acharya, J., Sahu, J. N., Mohanty, C. R. & Meikap, B. C. 2009 Removal of lead(II) from wastewater by activated carbon developed from Tamarind wood by zinc chloride activation. *Chemical Engineering Journal* **149** (1–3), 249–262.

ANA 2015 *Modifican los estándares Nacionales de Calidad de Agua y establecen disposiciones complementarias para su uso*. Retrieved from http://www.ana.gob.pe/sites/default/files/normatividad/files/ds-ndeg-015-2015-minam.pdf.

Ansari, F., Ghaedi, M., Taghdiri, M. & Asfaram, A. 2016 Application of ZnO nanorods loaded on activated carbon for ultrasonic assisted dyes removal: experimental design and derivative spectrophotometry method. *Ultrason Sonochem* **33**, 197–209.

Blanchard, G., Maunaye, M. & Martin, G. 1984 Removal of heavy metals from waters by means of natural zeolites. *Water Research* **18** (12), 1501–1507.

Chu, P. K. & Li, L. 2006 Characterization of amorphous and nanocrystalline carbon films. *Materials Chemistry and Physics* **96** (2–3), 253–277.

Copaciu, F., Opriş, O., Coman, V., Ristoiu, D., Niinemets, Ü. & Copolovici, L. 2013 Diffuse water pollution by Anthraquinone and Azo Dyes in environment importantly alters foliage volatiles, carotenoids and physiology in wheat (Triticum aestivum). *Water, Air, & Soil Pollution* **224** (3).

Cruz, G., Pirilä, M., Huuhtanen, M., Carrión, L., Alvarenga, E. & Keiski, R. L. 2012 Production of activated carbon from cocoa (*Theobroma cacao*) pod husk. *Journal of Civil & Environmental Engineering* **02** (02).

Cruz, G. J. F., Matějová, L., Pirilä, M., Ainassaari, K., Canepa, C. A., Solis, J. & Keiski, R. L. 2015 A comparative study on activated carbons derived from a broad range of agro-industrial wastes in removal of large-molecular-size organic pollutants in aqueous phase. *Water, Air, & Soil Pollution* **226** (7).

Dubinin, M. M. & Radushkevich, L. V. 1947 The equation of the characteristic curve of activated charcoal. *Proc. Acad. Sci. URSS Phys. Chem. Sect.* **55**, 331–337.

Fiol, N. & Villaescusa, I. 2008 Determination of sorbent point zero charge: usefulness in sorption studies. *Environmental Chemistry Letters* **7** (1), 79–84.

Freundlich, H. 1906 Uber die adsorption in Losungen. *Z. Phys. Chem.* **57** (1), 385–470.

Han, T. Y., Worsley, M. A., Baumann, T. F. & Satcher Jr., J. H. 2011 Synthesis of ZnO coated activated carbon aerogel by simple sol-gel route. *Journal of Materials Chemistry* **21** (2), 330–333.

Hor, K. Y., Chee, J. M. C., Chong, M. N., Jin, B., Saint, C., Poh, P. E. & Aryal, R. 2016 Evaluation of physicochemical methods in enhancing the adsorption performance of natural zeolite as low-cost adsorbent of methylene blue dye from wastewater. *Journal of Cleaner Production* **118**, 197–209.

Imamoglu, M. & Tekir, O. 2008 Removal of copper (II) and lead (II) ions from aqueous solutions by adsorption on activated carbon from a new precursor hazelnut husks. *Desalination* **228** (1–3), 108–113.

Kadirvelu, K. 2001 Removal of heavy metals from industrial wastewaters by adsorption onto activated carbon prepared from an agricultural solid waste. *Bioresource Technology* **76** (1), 63–65.

Kikuchi, Y., Qian, Q., Machida, M. & Tatsumoto, H. 2006 Effect of ZnO loading to activated carbon on Pb(II) adsorption from aqueous solution. *Carbon* **44** (2), 195–202.

Lagergren, S. 1898 About the theory of so-called adsorption of soluble substances. *K. Sven. Vetens. Handl.* **24** (4), 1–39.

Langmuir, I. 1918 The adsorption of gases on plane surfaces of glass, mica and platinum. *Journal of American Chemical Society* **40** (9), 1361–1403.

Lopez-Ramon, M. V., Stoeckli, F., Moreno-Castilla, C. & Carrasco-Marina, F. 1999 On the characterization of acidic and basic surface sites on carbons by various techniques. *Carbon* **37**, 1215–1221.

Manjunath, K., Lingaraju, K., Kumar, D., Nagabhushan, H., Samrat, D., Reddy, V. & Nagaraju, G. 2015 Electrochemical sensing of dopamine and antibacterial properties of ZnO nanoparticles synthesized from solution combustion method. *International Journal of Nanoscience* **14** (03).

Nagajyoti, P. C., Lee, K. D. & Sreekanth, T. V. M. 2010 Heavy metals, occurrence and toxicity for plants: a review. *Environmental Chemistry Letters* **8** (3), 199–216.

Ortiz-Ibarra, H., Casillas, N., Soto, V., Barcena-Soto, M., Torres-Vitela, R., de la Cruz, W. & Gomez-Salazar, S. 2007 Surface characterization of electrodeposited silver on activated carbon for bactericidal purposes. *J. Colloid Interface Sci.* **314** (2), 562–571.

Pirila, M., Cruz, G. J. F., Ainassaari, K., Gomez, M. M., Matejova, L. & Keiski, R. L. 2017 Adsorption of As(V), Cd(II) and Pb(II), in multicomponent aqueous systems using activated carbons. *Water Environ. Res.* **89** (9), 846–855.

Pirsaheb, M., Rezai, Z., Mansouri, A. M., Rastegar, A., Alahabadi, A., Sani, A. R. & Sharafi, K. 2015 Preparation of the activated carbon from India shrub wood and their application for methylene blue removal: modeling and optimization. *Desalination and Water Treatment* **57** (13), 5888–5902.

Rafatullah, M., Sulaiman, O., Hashim, R. & Ahmad, A. 2010 Adsorption of methylene blue on low-cost adsorbents: a review. *J. Hazard. Mater.* **177** (1–3), 70–80.

Rahman, Q. I., Ahmad, M., Misra, S. K. & Lohani, M. 2013 Effective photocatalytic degradation of rhodamine B dye by ZnO nanoparticles. *Materials Letters* **91**, 170–174.

Redlich, O. J. D. L. & Peterson, D. L. 1959 A useful adsorption isotherm. *J. Phys. Chem.* **63** (6), 1024–1024.

Roginsky, S. & Zeldovich, Y. 1934 The catalytic oxidation of carbon monoxide on manganese dioxide. *Acta Physicochim.* **1**, 554.

Saravanan, R., Gupta, V. K., Narayanan, V. & Stephen, A. 2013 Comparative study on photocatalytic activity of ZnO prepared by different methods. *Journal of Molecular Liquids* **181**, 133–141.

Sekar, M., Sakthi, V. & Rengaraj, S. 2004 Kinetics and equilibrium adsorption study of lead(II) onto activated carbon prepared from coconut shell. *J. Colloid Interface Sci.* **279** (2), 307–313.

Singh, C. K., Sahu, J. N., Mahalik, K. K., Mohanty, C. R., Mohan, B. R. & Meikap, B. C. 2008 Studies on the removal of Pb(II) from wastewater by activated carbon developed from Tamarind wood activated with sulphuric acid. *J. Hazard. Mater.* **153** (1–2), 221–228.

Smedley, P. L. & Kinniburgh, D. G. 2002 A review of the source, behaviour and distribution of arsenic in natural waters. *Applied Geochemistry* **17**, 517–568.

Sobana, N. & Swaminathan, M. 2007 Combination effect of ZnO and activated carbon for solar assisted photocatalytic degradation of Direct Blue 53. *Solar Energy Materials and Solar Cells* **91** (8), 727–734.

Srinivasan, N. R., Shankar, P. A. & Bandyopadhyaya, R. 2013 Plasma treated activated carbon impregnated with silver nanoparticles for improved antibacterial effect in water disinfection. *Carbon* **57**, 1–10.

Tao, X. & Xiaoqin, L. 2008 Peanut shell activated carbon: characterization, surface modification and adsorption of

Pb^{2+} from aqueous solution. *Chinese Journal of Chemical Engineering* **16** (3), 401–406.

Tran, H. N., You, S. J., Hosseini-Bandegharaei, A. & Chao, H. P. 2017 Mistakes and inconsistencies regarding adsorption of contaminants from aqueous solutions: a critical review. *Water Res.* **120**, 88–116.

Weber, W. J. & Morris, J. C. 1963 Kinetics of adsorption on carbon from solution. *J. Sanit. Eng. Div.* **89** (2), 31–60.

Zhang, S., Fu, R., Wu, D., Xu, W., Ye, Q. & Chen, Z. 2004 Preparation and characterization of antibacterial silver-dispersed activated carbon aerogels. *Carbon* **42** (15), 3209–3216.

First received 10 January 2018; accepted in revised form 5 April 2018. Available online 16 April 2018